Large-scale computation of wave energy converter arrays

Liu, Yingyi
Research Institute for Applied Mechanics, Kyushu University

Large-scale computation of wave energy converter arrays

Yingyi Liu
Kyushu University, liuyingyi@riam.kyushu-u.ac.jp

8.1 INTRODUCTION

This chapter is dedicated to the numerical modelling of wave energy converter (WEC) arrays. Deployment of WEC devices into arrays becomes a trend when the technology moves into the large-scale commercial exploitation stages, creating so-called "WEC farms". The arrays can be deployed in nearshore zones or those further offshore, depending on the type of the devices. One big advantage of "WEC farms" is that the devices can share some common infrastructures such as power substations, mooring systems and cables, which can significantly reduce the cost of construction and maintenance, as shown in Figure 8.1. In addition, the electricity generated by arrays of WECs can be far more stable than that generated by a single individual device. Wave farms of this nature are thereby beneficial to reduce the overall cost. The objective of optimising wave farm performance will be discussed extensively in Chapter 9.

Due to the fact that a WEC device in an array is not only subject to ambient incident waves, but also to those that have been reflected and radiated from the other WECs [124], an important issue that must be taken into account is the hydrodynamic interactions between the devices. In this chapter, we will first introduce the existing knowledge of the WEC array modelling methods in Section 8.2, and then present a hybrid methodology combining interaction theory (IT) and the boundary element method (BEM) in Sections 8.3–8.5. Evaluation of array properties are illustrated in Section 8.6 where a case study is given. The method described in this chapter is expected to be promising for a WEC farm of generic device geometries.

DOI: 10.1201/9781003198956-8

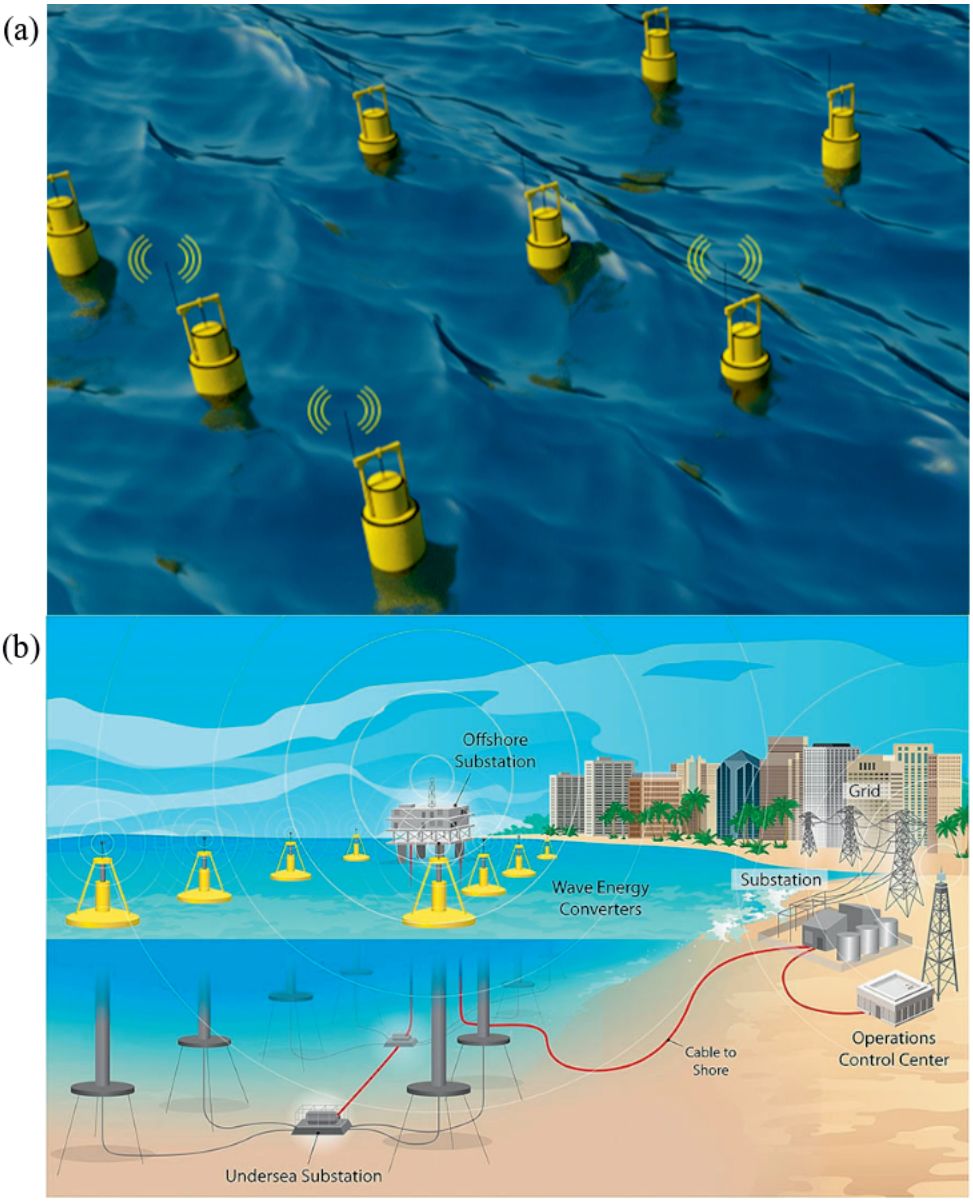

Figure 8.1: Artist's impression of a wave energy farm: (a) an array of point absorbers (artwork credit and copyright, 2018: Lu Wang, Ph.D.). This picture is taken from Ref. [876], under the Creative Commons Attribution 4.0 International License (http://creativecommons.org/licenses/by/4.0/); (b) the conceptual design of a wave farm. Illustration by Alfred Hicks, NREL.

8.2 REVIEW OF EXISTING ARRAY MODELLING METHODS

The theory for evaluating the power absorption of WEC arrays traces back to Refs. [97, 209, 224]. D. V. Evans [209] and J. Falnes [224] independently derived a general power absorption theory for arrays of oscillating bodies around 1979–1980. In the

earliest works, simplified theories were proposed to reduce the complexity of array interactions due to the limitations of computational technologies. Two of the representative simplified theories are: *point-absorber approximation* [97, 208, 209, 210, 224, 524], assuming that the device's characteristic length are small enough in comparison with the incident wave length, and *plane-wave approximation* [718, 523, 525, 525], assuming that the devices are widely spaced relative to the wave length. Refs. [524, 510] performed comparative studies on these approximations.

Beside quick approximations, exact theories were also developed, such as the multiple scattering method [591, 507, 508, 717] and the direct matrix method [389, 295, 393, 124, 530, 245]. The limitation of the first approach is that only expansions with explicit analytical expressions can be applicable; while in the latter approach, the advantages of the multiple scattering method and the numerical BEM can be combined to account for devices with complex geometries.

Kagemoto and Yue (1986) [389] developed an exact interaction theory based on multiple-scattering interaction theory [591] with the direct matrix method [740, 718, 527, 523], and applied it to axisymmetric bodies using a hybrid element method [859]. Goo and Yoshida (1990) [295] extended this method to bodies of complex shape by using the source panel method and the Green function in polar coordinates [71, 239, 362]. Further extensions were made to interaction theory in infinite-depth water by Peter and Meylan (2004) [632], and to hierarchical interaction theory with multiple layers by Kashiwagi (2000) [393]. Child and Venugopal (2010) [124] applied semi-analytical techniques to study optimal configurations of WEC arrays. McNatt et al. (2015) [530] developed a simplified method that can derive the diffraction transfer matrix (DTM) and the radiation characteristics (RC) from the standard output of wave potentials of a BEM solver. However, their method considers only the progressive mode and ignores the evanescent modes. Later, Flavia et al. (2018) [245] implemented the method of [295] on the open-source BEM code Nemoh [46] and derived general identities to water-wave multiple-scattering problems [246]. Liu et al. (2021) [457] derived the formulations for evaluating the DTM and RC using the hybrid source and dipole method, increasing accuracy over the methods described in Refs. [295] and [245].

Exact theories on multiple bodies have been applied to various fields, such as the interconnected multi-moduled floating offshore structure [111], ice-floes in the marginal ice zone [632, 69], very-large floating structures [394], and, recently, arrays of wave energy converters [298, 877, 873], in which analytical approaches or semi-analytical approaches applying multiple-scattering interaction theory have been used extensively.

8.3 INTERACTION THEORY

8.3.1 The concept of partial waves

Prior to presenting the interaction theory of multiple floating bodies, for convenience, the concept of "partial waves" needs to be introduced. In a finite-sized array of floating bodies, the wave velocity potential can be expressed as a scalar product between a vector of complex coefficients and a vector of partial cylindrical wave

components [529, 245]. As discussed in Section 2.2.1, the incident wave potential to body j involves the incoming wave solutions to the Laplace equation, subjecting it to a set of boundary conditions in polar coordinates

$$\begin{aligned}\phi_j^I(r_j,\theta_j,z_j) = \sum_{q=-\infty}^{\infty} \Bigg[\left(A_j^I\right)_{0q} \frac{\cosh k\left(z_j+d\right)}{\cosh k_0 d} J_q\left(kr_j\right) \\ + \sum_{l=1}^{\infty} \left(A_j^I\right)_{lq} \cos k_l\left(z_j+d\right) I_q\left(k_l r_j\right) \Bigg] e^{iq\theta_j},\end{aligned} \tag{8.1}$$

where J_q is the Bessel function of the first kind of order q, and I_q is the modified Bessel function of the first kind of order q. The scattered and the radiated wave potentials involve the outgoing wave solutions

$$\begin{aligned}\phi_j^S(r_j,\theta_j,z_j) = \sum_{m=-\infty}^{\infty} \Bigg[\left(A_j^S\right)_{0m} \frac{\cosh k\left(z_j+d\right)}{\cosh k_0 d} H_m^{(1)}\left(kr_j\right) \\ + \sum_{n=1}^{\infty} \left(A_j^S\right)_{nm} \cos k_n\left(z_j+d\right) K_m\left(k_n r_j\right) \Bigg] e^{im\theta_j},\end{aligned} \tag{8.2}$$

$$\begin{aligned}\phi_j^{R,p}(r_j,\theta_j,z_j) = \sum_{m=-\infty}^{\infty} \Bigg[\left(R_j^p\right)_{0m} \frac{\cosh k\left(z_j+d\right)}{\cosh k_0 d} H_m^{(1)}\left(kr_j\right) \\ + \sum_{n=1}^{\infty} \left(R_j^p\right)_{nm} \cos k_n\left(z_j+d\right) K_m\left(k_n r_j\right) \Bigg] e^{im\theta_j}.\end{aligned} \tag{8.3}$$

where $\boldsymbol{x}_j = (r_j,\theta_j,z_j)$ represents the polar coordinates of the field point $\boldsymbol{x}_j$ in the fluid domain; $H_m^{(1)}$ is the Hankel function of the first kind of order m; K_m is the modified Bessel function of the second kind of order m; and p stands for the pth body rigid mode. Note that the wavenumber k is the positive root of the water wave dispersion equation Eq. (2.54); k_n $(n=1,2,...)$ satisfies Eq. (2.55), characterising the evanescent modes of the eigenfunction expansion. Eqs. (8.1), (8.2), and (8.3) can be written in a compact vector form

$$\phi_j^I = \{A_j^I\}^T\{\psi_j^I\};\ \ \phi_j^S = \{A_j^S\}^T\{\psi_j^S\};\ \ \phi_j^{R,p} = \{A_j^{R,p}\}^T\{\psi_j^S\}, \tag{8.4}$$

where the superscript T represents the transpose operator for a matrix or vector, the curly bracket stands for a vector; and A_j^I, A_j^S and $A_j^{R,p}$ are the complex incident, scattered and radiated vectors of partial wave coefficients. Herein, indexes (l,q) are associated with incident waves and (n,m) with outgoing waves. The vectors of the incident and scattered cylindrical functions are respectively

$$\left\{\psi_j^I\right\}_{lq} = \begin{cases} \frac{\cosh k\left(z_j+h\right)}{\cosh kh} J_q\left(kr_j\right) e^{\mathrm{i}q\theta_j}, & l=0 \\ \cos k_l\left(z_j+h\right) I_q\left(k_l r_j\right) e^{\mathrm{i}q\theta_j}, & l\geq 1 \end{cases}, \tag{8.5}$$

$$\left\{\psi_j^S\right\}_{nm} = \begin{cases} \frac{\cosh k\left(z_j+h\right)}{\cosh kh} H_m^{(1)}(kr_j) e^{\mathrm{i}m\theta_j}, & n=0 \\ \cos k_n\left(z_j+h\right) K_m\left(k_n r_j\right) e^{\mathrm{i}m\theta_j}, & n\geq 1 \end{cases}. \tag{8.6}$$

It is noted that the first terms of the incident and scattered cylindrical functions represent the propagating mode, while the rest of the terms are associated with evanescent modes.

8.3.2 Ambient incident plane waves

Let us consider a long-crested incident wave propagating to the positive x-direction, transmitting with a small amplitude A, a heading angle β measured from the positive x-axis, and a wave number k, in water with a finite depth of h. The ambient wave potential incident to body j can be written as

$$\phi_j^A(x_j, y_j, z_j) = -\frac{igA}{\omega}\frac{\cosh k(z_j+h)}{\cosh kh} e^{ik(x_j\cos\beta + y_j\sin\beta)}. \tag{8.7}$$

By means of the polar coordinates, Eq. (8.7) can be expressed relative to body j

$$\phi_j^A(r_j, \theta_j, z_j) = -\frac{igA}{\omega}\frac{\cosh k(z+h)}{\cosh kh} I_j e^{ikr_j\cos(\theta_j-\beta)}. \tag{8.8}$$

where $I_j = e^{ik(x_j\cos\beta + y_j\sin\beta)}$ is a phase factor dependent on body j, and r_j is the radial coordinate of the point $\boldsymbol{x}_j = (r_j, \theta_j, z_j)$ in the local coordinate system of body j. Using an identity [8], Eq. (8.8) can be further expanded as a summation of partial cylindrical waves incident on the body j

$$\phi_j^A(r_j, \theta_j, z_j) = -\frac{igA}{\omega}\frac{\cosh k(z+h)}{\cosh kh} I_j \sum_{q=-\infty}^{\infty} J_q(kr_j) e^{iq(\pi/2+\theta_j-\beta)}. \tag{8.9}$$

In comparison with Eq. (8.1), Eq. (8.9) reduces to

$$\phi_j^I(x_j, y_j, z_j) = \{a_j^I\}^T\{\psi_j^I\}, \tag{8.10}$$

where the expansion coefficients are

$$\left\{a_j^l\right\}_{lq} = \begin{cases} -i\frac{gA}{\omega} e^{ik_0\left(x_j\cos\beta + y_j\sin\beta\right)} e^{iq(\pi/2-\beta)}, & l=0 \\ 0 & l\geq 1 \end{cases}. \tag{8.11}$$

8.3.3 Solution of the partial wave coefficients

The complex expansion coefficients A_j^I, A_j^S, and $A_j^{R,p}$ are the only unknowns to be solved for an array of bodies. The primary task in this subsection is to find a relationship between these unknown coefficients and the existing information. We deal with the diffraction and radiation problems separately, as in Refs. [530, 245], rather than treating them simultaneously as a whole (e.g., [124]).

In Eq. (8.4), the scattered wave potential of body j amongst an array of bodies is expressed as the scalar product of scattered coefficients and outgoing partial wave components. Using Graf's addition theorem [8], it is straightforward to obtain

$$H_m(k_0r_i)e^{im\theta_i} = \sum_{q=-\infty}^{\infty} H_{m+q}(k_0L_{ij}) J_q(k_0r_j) e^{i\left[\alpha_{ij}(m+q)+q\left(\pi-\theta_j\right)\right]}, \tag{8.12}$$

$$K_m(k_nr_i)e^{im\theta_i} = \sum_{q=-\infty}^{\infty} K_{m+q}(k_nL_{ij}) I_q(k_nr_j) e^{i\left[\alpha_{ij}(m+q)+q\left(\pi-\theta_j\right)\right]}. \tag{8.13}$$

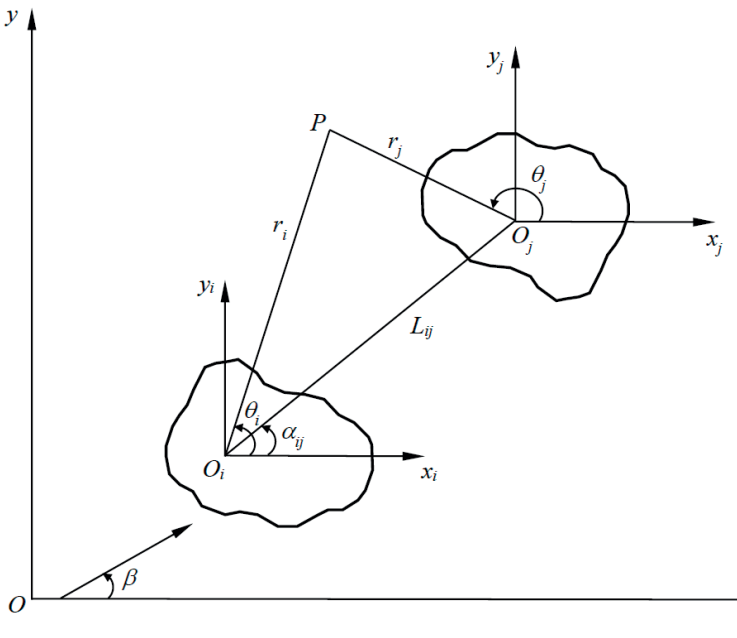

Figure 8.2: Schematic of the local and global coordinate systems.

where L_{ij} is the distance between the centres (origins of the local coordinate systems) of body i and j; α_{ij} is the angle at body i between the positive x-direction and the line joining the centre of i to that of j in an anti-clockwise direction (see Figure 8.2) [121]. In order to apply Graf's addition theorem, it is necessary to assume here that the circumscribing cylinder of each body does not overlap vertically with the other's. Eqs. (8.12) and (8.13) hold true for any integer m, and any non-negative integer n, when $r_j \leq L_{ij}$. The two formulae are the basis to derive a coordinate transformation matrix $[T_{ij}]$, for every pair of i, j except $i = j$:

$$[T_{ij}]_{nn}^{mq} = \begin{cases} H_{m-q}(k_0 L_{ij}) \mathrm{e}^{\mathrm{i}\alpha_{ij}(m-q)}, & n = 0 \\ K_{m-q}(k_n L_{ij}) \mathrm{e}^{\mathrm{i}\alpha_{ij}(m-q)} (-1)^q, & n \geq 1 \end{cases}. \tag{8.14}$$

Note that the square bracket in this chapter indicates a matrix. Eq. (8.14) can be used to express the scattered partial wave components in terms of the incident partial wave components:

$$\{\psi_i^S\} = [T_{ij}]\{\psi_j^I\}. \tag{8.15}$$

According to Eq. (8.4), the scattered waves from body i can be expressed as the incident waves to body j:

$$\phi_i^S(r_i, \theta_i, z_i) = \{A_i^S\}^T [T_{ij}]\{\psi_j^I\}. \tag{8.16}$$

In this way, the total wave potentials incident to body j can be written as a summation of the ambient incident wave and all scattered waves from the other bodies

$$\begin{aligned}\phi_j^I(r_j,\theta_j,z_j) &= \phi_j^A(r_j,\theta_j,z_j) + \sum_{\substack{i=1\\ i\neq j}}^{N_B} \{A_i^S\}^T [T_{ij}]\{\psi_j^I\} \\ &= (\{a_j^I\}^T + \sum_{\substack{i=1\\ i\neq j}}^{N_B} \{A_i^S\}^T [T_{ij}]) \cdot \{\psi_j^I\}, \quad (j=1,2,...,N_B),\end{aligned} \tag{8.17}$$

where N_B stands for the number of bodies in the array.

The incident and scattered partial waves can be related by a linear operator, termed DTM $[D_j]$. It transfers the incident partial waves to the corresponding scattered partial waves. The element $[D_j]_{nl}^{mq}$ is defined as the amplitude of the $[n(2M+1)+m+1]^{\text{th}}$ scattered partial wave potential due to a single unit-amplitude incidence of the $[l(2Q+1)+q+1]^{\text{th}}$ mode on body j, where M and Q represent the number of truncation terms in m and q, respectively. Therefore, it is straightforward to write the scattered wave potential from body j as

$$\phi_j^S(r_j,\theta_j,z_j) = (\{a_j^I\}^T + \sum_{\substack{i=1\\ i\neq j}}^{N_B} \{A_i^S\}^T [T_{ij}]) \cdot [D_j]^T \{\psi_j^S\}, \quad (j=1,2,...,N_B). \tag{8.18}$$

The combination of Eqs. (8.4) and (8.18) yields a new equation. Cancelling the common vector of scattered partial waves and transposing both of the left- and right-hand sides of the equation results in

$$\{A_j^S\} = [D_j] \cdot (\{a_j^I\} + \sum_{\substack{i=1\\ i\neq j}}^{N_B} [T_{ij}]^T \{A_i^S\}), \quad (j=1,2,...,N_B). \tag{8.19}$$

Following a similar method, the equation for the radiation problem is

$$\{A_j^{R,i,p}\} = [D_j] \cdot (\{a_j^{R,i,p}\} + \sum_{\substack{t=1\\ t\neq j}}^{N_B} [T_{tj}]^T \{A_t^{R,i,p}\}), \quad (j=1,2,...,N_B), \tag{8.20}$$

where $\{a_j^{R,i,p}\}$ are the expansion coefficients of the radiated wave incident on body j, generated by the unitary motion of body i in its p^{th} degree of freedom:

$$\left\{a_j^{R,i,p}\right\} = \begin{cases} 0, & i=j \\ [T_{ij}]^T \cdot \{R_i^p\}, & i\neq j \end{cases}, \tag{8.21}$$

where $\{R_i^p\}$ is termed as RC. Note that Eqs. (8.19) and (8.20) are expressed for each body. It is thereby possible to assemble a large linear algebraic system involving all the bodies in the array to solve the scattered partial wave coefficients.

8.3.4 Wave excitation forces and hydrodynamic quantities

Wave forces can be calculated using matrix manipulation after the scattered partial wave coefficients are obtained. Based on Eqs. (8.17) and (8.18), the wave excitation

force can be calculated by integrating the hydrodynamic pressure over the immersed body surface:

$$F_{j,p}^{E} = \mathrm{i}\omega\rho \iint_{S_B^j} \left(\phi_j^I + \phi_j^S\right) n_{j,p} \mathrm{d}S = \mathrm{i}\omega\rho \left(\left\{a_j^I\right\}^T + \sum_{\substack{i=1 \\ i\neq j}}^{N_B} \left\{A_i^S\right\}^T [T_{ij}] \right) \times \iint_{S_B^j} \left(\left\{\psi_j^I\right\} + [D_j]^T \left\{\psi_j^S\right\} \right) n_{j,p} \mathrm{d}S, \quad (p = 1,2,...,6, j = 1,2,...,N_B) \tag{8.22}$$

where $F_{j,p}^{E}$ is interpreted as the excitation force in the p^{th} DoF of body j, and $n_{j,p}$ is the p^{th} component of the normal vector on the immersed body surface. By defining a new linear operator-force transfer matrix as

$$\left\{G_{j,p}^{E}\right\} = \mathrm{i}\omega\rho \iint_{S_B^j} \left(\left\{\psi_j^I\right\} + [D_j]^T \left\{\psi_j^S\right\} \right) n_{j,p} \mathrm{d}S, \tag{8.23}$$

and the overall expansion coefficients of the total waves incident to body j, which consists of the ambient incident wave and all the scattered waves from neighbouring bodies as

$$\left\{\eta_j^E\right\} = \left\{a_j^I\right\}^T + \sum_{\substack{i=1 \\ i\neq j}}^{N_B} \left\{A_i^S\right\}^T [T_{ij}], \tag{8.24}$$

calculation of the wave excitation force on body j can be simplified in the following matrix form:

$$F_{j,p}^{E} = \left\{\eta_j^E\right\} \left\{G_{j,p}^{E}\right\}. \tag{8.25}$$

Following a similar method, the wave radiation force on body j can be evaluated as

$$F_{j,t}^{R,i,p} = \begin{cases} \left\{\eta_j^{R,i,p}\right\} \left\{G_{j,t}^{E}\right\}, & i \neq j \\ \mathrm{i}\rho\left(a_{j,p} + \omega b_{j,p}\right) + \left\{\eta_j^{R,i,t}\right\} \left\{G_{j,t}^{E}\right\}, & i = j \end{cases} \tag{8.26}$$

where $a_{j,p}$ and $b_{j,p}$ are the added mass and the radiation damping of body j in the p^{th} DoF due to its own unitary motion in the same mode when the body is in isolation; the overall expansion coefficient in association with the force transfer matrix is

$$\left\{\eta_j^{R,i,p}\right\} = \left\{a_j^{R,i,p}\right\}^T + \sum_{\substack{t=1 \\ t\neq j}}^{N_B} \left\{A_t^{R,i,p}\right\}^T [T_{tj}]. \tag{8.27}$$

Note that $F_{j,t}^{R,i,p}$ is interpreted as the radiation force of body j in the t^{th} DoF due to the p^{th} DoF motion of body i. Correspondingly, the added mass and the radiation damping of a body can then be obtained by decomposition of the complex radiation force into real and imaginary parts.

Figure 8.3 gives a comparison between different methods in calculating the wave forces on arrays of bodies, which shows a high-degree match between them. This numerical case consists of an array of 4 truncated cylinders and the details of the layout

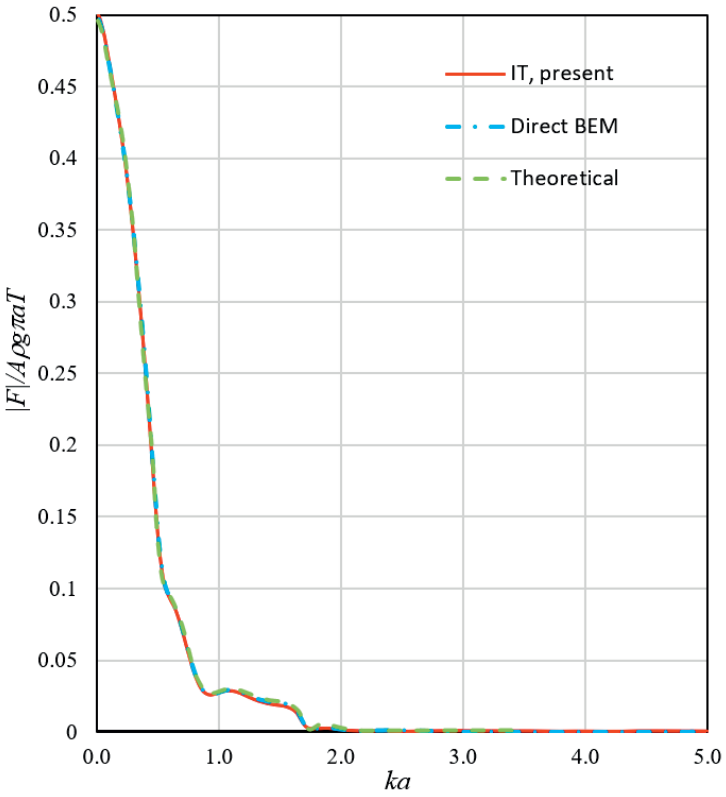

Figure 8.3: Variations of the heave excitation force on Cylinder 1 of an array of 4 truncated vertical cylinders with radius a, draught $T = 2a$, in a water depth of $h = 4a$ with each cylinder placed at the vertex of a square of side length $4a$ for an incident wave heading angle of $\beta = \pi/4$.

are given in Ref. [717]. The "Direct BEM" denotes the complete BEM method based on mixed sources and dipoles as described in Section 2.2.2 of Chapter 2. "Theoretical" denotes the result calculated by Ref. [717]. Although "Direct BEM" is not limited to regular geometries, the computational cost is much more expensive than the "Theoretical" method. In contrast with the other two methods, the present method, based on interaction theory, provides a compromise option for arrays of complex geometries.

8.3.5 Motion responses

Given the body specifications, the power-take-off (PTO) characteristics, the mooring system properties and the wave loads, the motion equation of body j can be constructed as

$$\left\{-\omega^2\left([M]+[A_{\mathrm{m}}]\right)-\mathrm{i}\omega\left([B_{\mathrm{rad}}]+[B_{\mathrm{pto}}]\right)+\left([K_{\mathrm{s}}]+[K_{\mathrm{pto}}]+[K_{\mathrm{moor}}]\right)\right\}\{X\}=\{F^E\}, \tag{8.28}$$

where $[M]$ is the device mass matrix, $[A_{\mathrm{m}}]$ and $[B_{\mathrm{rad}}]$ the device added mass and the radiation damping matrices, $[B_{\mathrm{pto}}]$ and $[K_{\mathrm{pto}}]$ the mechanical damping and the stiffness matrices related to the PTO system, $[K_{\mathrm{s}}]$ the hydrostatic restoring matrix, $[K_{\mathrm{moor}}]$ the mooring stiffness matrix, $\{X\}$ the displacement vector, and $\{F^E\}$ the wave excitation force vector. Note that all the above matrices or vectors are of body j. For brevity, the subscript j is omitted in Eq. (8.28).

8.4 LINEAR OPERATOR MATRICES

A linear operator matrix refers to a matrix that relates two different physical variables in interaction theory within the framework of the linear water wave (see Section 2.1.1.2 of Chapter 2). To simulate the wave interactions between an array of bodies, an essential characteristic is that the linear operators are only determined by a single body in isolation. The existence of linear operators facilitates multi-body computations via the matrix form based on the direct matrix method.

8.4.1 Diffraction transfer matrix

A diffraction transfer matrix (DTM) represents the scattering properties of a body and is solved from the boundary value problem (Eq. 8.43 or Eq. 8.45) for the body in isolation. Technically speaking, DTM transforms a vector of incident, cylindrical, partial-wave coefficients into a vector of outgoing, partial-wave coefficients representing waves scattered by the body [389, 530].

8.4.1.1 Alternative method I

The 1st linear operator, the DTM of a specific floating body, as mentioned in Eq. (8.18), can be constructed by considering the wave diffraction when it is in isolation. The scattered potential of a single floating body in a partial incident wave of mode (l,q) without the presence of other bodies can be expressed as

$$\begin{aligned}\left\{\varphi_j^S\left(r_j,\theta_j,z_j\right)\right\}_{l,q} &= \frac{\cosh k\left(z_j+h\right)}{\cosh kh}\sum_{m=-\infty}^{\infty}\left[D_j\right]_{0,m}^{l,q}H_m^{(1)}\left(kr_j\right)e^{\mathrm{i}m\theta_j}\\ &+\sum_{n=1}^{\infty}\cos k_n\left(z_j+h\right)\sum_{m=-\infty}^{\infty}\left[D_j\right]_{n,m}^{l,q}K_m\left(k_nr_j\right)e^{\mathrm{i}m\theta_j}\end{aligned} \tag{8.29}$$

where $D_{0m}^{j,lq}$ and $D_{nm}^{j,lq}$ are scattered complex coefficients as well as the DTM elements. The scattered potential at a field point in the fluid domain (other than the body surface) can be determined by the following equation:

$$\begin{aligned}\left\{\varphi_j^S\left(\boldsymbol{x}_j\right)\right\}_{l,q} = -\frac{1}{4\pi}\Bigg\{&\iint_{S_B^j}\left\{\varphi_j^S\left(\boldsymbol{\xi}_j\right)\right\}_{l,q}\frac{\partial G(\boldsymbol{x}_j;\boldsymbol{\xi}_j)}{\partial n(\boldsymbol{\xi}_j)}\mathrm{d}S_{\boldsymbol{\xi}_j}\\ &+\iint_{S_B^j}G\left(\boldsymbol{x}_j;\boldsymbol{\xi}_j\right)\frac{\partial\left\{\psi_j^I\left(\boldsymbol{\xi}_j\right)\right\}_{l,q}}{\partial n_\xi}\mathrm{d}S_{\boldsymbol{\xi}_j}\Bigg\}.\end{aligned} \tag{8.30}$$

Substituting Eq. (8.46) into Eq. (8.30) and comparing Eq. (8.29) with Eq. (8.30) yields

$$[D_j]^{l,q}_{0,m} = -\frac{i}{2}C_0 \cosh kh \iint_{S_B^j} \left[\{\varphi_j^S\}_{l,q}\frac{\partial}{\partial n} + \frac{\partial\{\psi_j^I\}_{l,q}}{\partial n}\right]\left[J_m(kR_j)\cosh k(\zeta_j+h)e^{-\mathrm{i}m\Theta_j}\right]\mathrm{d}S_{\boldsymbol{\xi}_j}, \tag{8.31}$$

$$[D_j]^{l,q}_{n,m} = -\frac{1}{\pi}C_n \iint_{S_B^j} \left[\{\varphi_j^S\}_{l,q}\frac{\partial}{\partial n} + \frac{\partial\{\psi_j^I\}_{l,q}}{\partial n}\right]\left[I_m(k_nR_j)\cos k_n(\zeta_j+h)e^{-\mathrm{i}m\Theta_j}\right]\mathrm{d}S_{\boldsymbol{\xi}_j}. \tag{8.32}$$

The unknown wave scattering potential φ^S_{jlq} in Eq. (8.15) and Eq. (8.16) on the body surface can be solved from the following boundary integral equation:

$$2\pi\{\varphi_j^S(\boldsymbol{x}_j)\}_{l,q} + \iint_{S_B^j}\{\varphi_j^S(\boldsymbol{\xi}_j)\}_{l,q}\frac{\partial G(\boldsymbol{x}_j;\boldsymbol{\xi}_j)}{\partial n(\boldsymbol{\xi}_j)}\mathrm{d}S_{\boldsymbol{\xi}_j} = -\iint_{S_B^j}\frac{\partial\{\psi_j^I(\boldsymbol{\xi}_j)\}_{l,q}}{\partial n_\xi}G(\boldsymbol{x}_j;\boldsymbol{\xi}_j)\mathrm{d}S_{\boldsymbol{\xi}_j}. \tag{8.33}$$

8.4.1.2 Alternative method II

Refs. [395, 393] employed a different boundary integral equation to solve the total wave diffraction potential φ_j^D, i.e.,

$$2\pi\{\varphi_j^D(\boldsymbol{x}_j)\}_{l,q} + \iint_{S_B^j}\{\varphi_j^D(\boldsymbol{\xi}_j)\}_{l,q}\frac{\partial G(\boldsymbol{x}_j;\boldsymbol{\xi}_j)}{\partial n(\boldsymbol{\xi}_j)}\mathrm{d}S_{\boldsymbol{\xi}_j} = 4\pi\{\psi_j^I(\boldsymbol{x}_j)\}_{l,q}, \tag{8.34}$$

from which the wave scattering potential φ_j^S at a field point in the fluid domain can easily be obtained by subtracting the incident partial wave component

$$\{\varphi_j^S(\boldsymbol{x}_j)\}_{l,q} = \{\varphi_j^D(\boldsymbol{x}_j)\}_{l,q} - \{\psi_j^I(\boldsymbol{x}_j)\}_{l,q} = -\frac{1}{4\pi}\iint_{S_B^j}\{\varphi_j^D(\boldsymbol{\xi}_j)\}_{l,q}\frac{\partial G(\boldsymbol{x}_j;\boldsymbol{\xi}_j)}{\partial n(\boldsymbol{\xi}_j)}\mathrm{d}S_{\boldsymbol{\xi}_j}. \tag{8.35}$$

Given the unknown wave scattering potential, the DTM elements can be found from Eqs. (8.29), (8.35) and (8.46):

$$[D_j]^{l,q}_{0,m} = -\frac{\mathrm{i}}{2}C_0\cosh kh\iint_{S_B^j}[\{\varphi_j^S\}_{l,q}+\{\varphi_j^I\}_{l,q}]\frac{\partial}{\partial n}[J_m(kR_j)\cosh k(\zeta_j+h)\mathrm{e}^{-\mathrm{i}m\Theta_j}]\mathrm{d}S, \tag{8.36}$$

$$[D_j]^{l,q}_{0,m} = -\frac{1}{\pi}C_n\iint_{S_B^j}[\{\varphi_j^S\}_{l,q}+\{\varphi_j^I\}_{l,q}]\frac{\partial}{\partial n}[I_m(k_nR_j)\cosh k_n(\zeta_j+h)\mathrm{e}^{-\mathrm{i}m\Theta_j}]\mathrm{d}S. \tag{8.37}$$

8.4.1.3 Comparison of accuracy and efficiency

In general, the accuracy of the two alternative methods is similar. However, there are cases (e.g., geometries with sharp corners) when Method II performs better than Method I. This is because at the right-hand side of the boundary integral equations, the integration of the normal derivative of the incident wave potential over the body

surface in Method I might have a larger cumulative numerical error than simple evaluation of the incident partial wave potential at a single field point in Method II. In addition, Method II is also superior to its counterpart in terms of computational efficiency as the right-hand side is faster to evaluate. This advantage may not be noticeable in single-body computations, but when it comes to a multi-body problem, the difference is remarkable. Ref. [457] compares the computational time for per-frequency DTM computation, showing that Method II is far more efficient than Method I when the truncation number of modes increases.

As an example, Figure 8.4 shows a comparison between the two alternative methods in calculating the DTM terms. McNatt et al. (2015) denotes the results given in Ref. [530]. Generally, there is a good level of agreement between the two methods in calculating both the real and the imaginary parts. However, it can be noticed that Method II performs slightly better than Method I in approaching the results of McNatt et al. (2015). Furthermore, the computation time of Method I in this numerical case is *more than ten times* that of Method II.

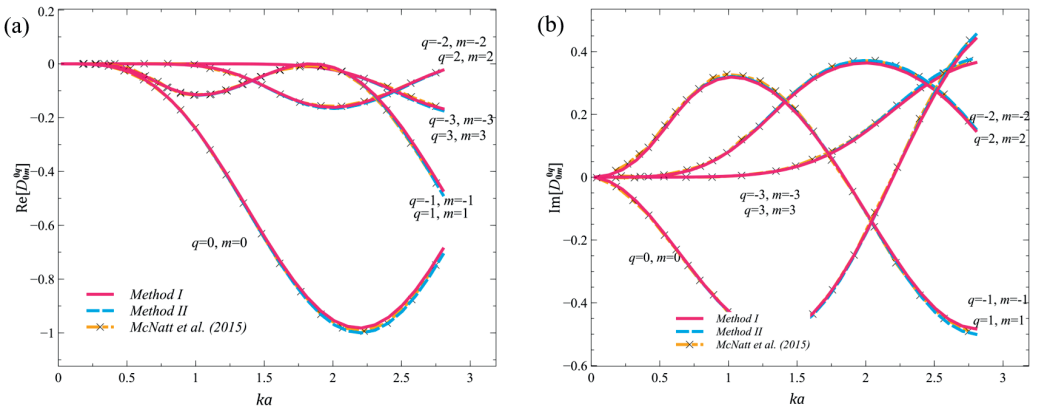

Figure 8.4: DTM progressive terms for a circular cylinder of 3 m radius, 6 m draft in a 10 m water depth, a comparison between Method I and Method II: (a) real part; (b) imaginary part. This figure is adapted from Ref. [457].

8.4.2 Radiation characteristics

Let us derive the expressions for the 2nd linear operator, the RC, as mentioned in Eq. (8.21). Physically, RC characterises the way in which a floating body radiates waves. The wave radiation potential $\{\varphi_j^{R,k}\}$ away from a single floating body of mode (n,m) without the influence of other bodies can be constructed as

$$\begin{aligned}\varphi_j^{R,p}(r_j,\theta_j,z_j) = &\frac{\cosh k(z_j+h)}{\cosh kh}\sum_{m=-\infty}^{\infty}\{R_j^p\}_{0,m}H_m^{(1)}(kr_j)\,\mathrm{e}^{\mathrm{i}m\theta_j}\\ &+\sum_{n=1}^{\infty}\cos k_n(z_j+h)\sum_{m=-\infty}^{\infty}\{R_j^p\}_{n,m}K_m(k_nr_j)\,\mathrm{e}^{\mathrm{i}m\theta_j},\end{aligned} \tag{8.38}$$

The radiation potential at a field point in the fluid domain (other than the body surface) can be determined by the following equation:

$$\varphi_j^{R,p}(\boldsymbol{x}_j) = -\frac{1}{4\pi}\left\{\iint_{S_B^j} \varphi_j^{R,p}(\boldsymbol{\xi}_j)\frac{\partial G(\boldsymbol{x}_j;\boldsymbol{\xi}_j)}{\partial n(\boldsymbol{\xi}_j)}\mathrm{d}S_{\boldsymbol{\xi}_j} - \iint_{S_B^j} n_{j,p}G(\boldsymbol{x}_j;\boldsymbol{\xi}_j)\,\mathrm{d}S_{\boldsymbol{\xi}_j}\right\}. \tag{8.39}$$

combining Eqs. (8.38), (8.39) and (8.46) leads to the following expressions of the RC elements:

$$\{R_j^p\}_{0,m} = -\frac{\mathrm{i}}{2}C_0\cosh kh\iint_{S_B^j}(\varphi_j^{R,p}\frac{\partial}{\partial n} - n_{j,p})[J_m(kR_j)\cosh k(\zeta_j+h)\mathrm{e}^{-\mathrm{i}m\Theta_j}]\mathrm{d}S, \tag{8.40}$$

$$\{R_j^p\}_{n,m} = -\frac{1}{\pi}C_n\iint_{S_B^j}(\varphi_j^{R,p}\frac{\partial}{\partial n} - n_{j,p})[I_m(k_nR_j)\cosh k_n(\zeta_j+h)\mathrm{e}^{-\mathrm{i}m\Theta_j}]\mathrm{d}S. \tag{8.41}$$

In Eq. (8.22) and Eq. (8.23), the unknown wave radiation potential $\varphi_j^{R,k}$ is solved from the following boundary integral equation:

$$2\pi\varphi_j^{R,p}(\boldsymbol{x}_j) + \iint_{S_B^j}\varphi_j^{R,p}(\boldsymbol{\xi}_j)\frac{\partial G(\boldsymbol{x}_j;\boldsymbol{\xi}_j)}{\partial n_\xi}\mathrm{d}S = \iint_{S_B^j} n_{j,p}G(\boldsymbol{x}_j;\boldsymbol{\xi}_j)\,\mathrm{d}S. \tag{8.42}$$

Figure 8.5 verifies the present method for calculating the RC progressive terms, by comparing the results given respectively in Refs. [245] and [530]. Good agreement is found between the three methods in all the RC terms shown. Furthermore, the values of RC terms of two additive inverse modes (e.g., $m=-1$ and $m=1$) are exactly the opposite; whereas the values of DTM terms of two such modes are exactly the same (see Figure 8.4).

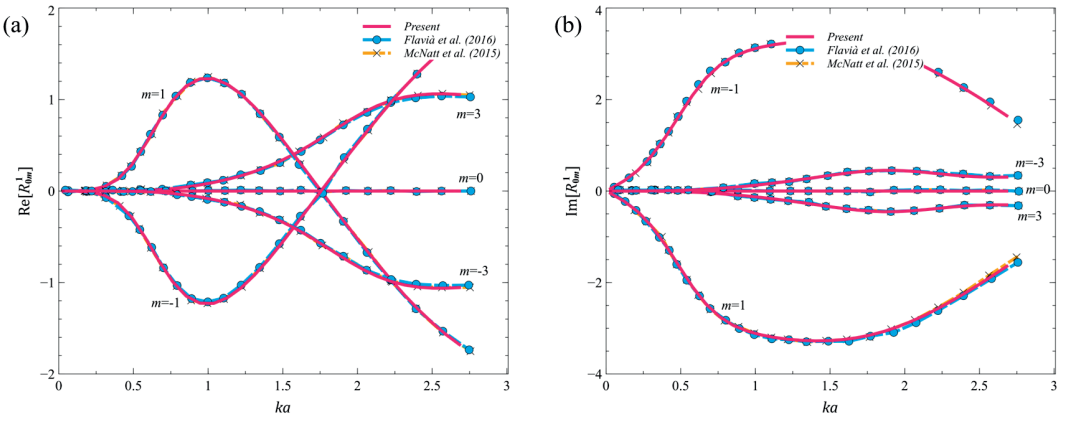

Figure 8.5: RC progressive terms for a cube box of 6 m side, 6 m draft moving in surge in a 10 m water depth: (a) real part and (b) imaginary part. This figure is taken from Ref. [457], under the Creative Commons Attribution 4.0 International License (http://creativecommons.org/licenses/by/4.0/).

8.4.3 Force transfer matrix

The 3rd linear operator, the force transfer matrix (FTM) $\{G^E_{j,p}\}$, given in Eq. (8.23), transforms a vector of incident partial cylindrical wave coefficients into forces (either diffraction or radiation) on a floating body. The idea of FTM was first introduced by McNatt et al. (2015) [530]. The elements of an FTM can be determined using the BEM (as introduced in Section 8.5) by integrating the hydrodynamic pressure (indeed, the diffraction or radiation potential) due to a partial wave.

8.5 BOUNDARY INTEGRAL EQUATIONS FOR PARTIAL WAVES

Wave radiation and diffraction of multiple floating bodies can be solved within the limits of potential flow theory, as discussed extensively in Section 2.2.2 of Chapter 2. Based on the assumption that the fluid is inviscid, incompressible, and with an irrotational motion, the fluid flow can be described by an ideal velocity potential satisfying the Laplace equation. However, the difference with Chapter 2 is that, in this section, partial wave potentials are considered instead of the incident plane wave.

8.5.1 Indirect approach

The indirect approach is based on the source formulation, which means that only sources are distributed on the immersed body surface. An isolated floating body is considered by adopting the polar coordinate system, the partial scattered wave potential should satisfy the following boundary integral equation:

$$2\pi\{\sigma^S_j(\boldsymbol{x}_j)\}_{l,q} + \iint_{S^j_B} \{\sigma^S_j(\boldsymbol{\xi}_j)\}_{l,q} \frac{\partial G(\boldsymbol{x}_j;\boldsymbol{\xi}_j)}{\partial n(\boldsymbol{x}_j)} \mathrm{d}S_{\boldsymbol{\xi}_j} = V_{\mathrm{n}}(\boldsymbol{x}_j), \tag{8.43}$$

where σ^S_j is the source strength and $G(\boldsymbol{x}_j;\boldsymbol{\xi}_j)$ is the free-surface Green's function. At the right-hand side of Eq. (8.43), the Neumann boundary condition prescribes the normal velocity of the fluid on the immersed and impermeable body surface:

$$V_{\mathrm{n}}(\boldsymbol{x}_j) = \begin{cases} n_{j,p}(\boldsymbol{x}_j), & p = 1,2,...,6 \\ -\frac{\partial\{\psi^I_j(\boldsymbol{x}_j)\}}{\partial n(\boldsymbol{x}_j)}, & p = 7 \end{cases} \tag{8.44}$$

in which $n_{j,p}$ is defined in Eq. (8.22). Note that in Eq. (8.43) and Eq. (8.44), the body boundary condition and the normal derivative are applied at the field point $\boldsymbol{x}_j = (r_j, \theta_j, z_j)$ rather than at the source point $\boldsymbol{\xi}_j = (R_j, \Theta_j, \zeta_j)$.

8.5.2 Direct approach

The direct approach is based on the potential formulation, involving both the sources and dipoles. Unlike the indirect approach, the wave potential can be directly solved from the boundary integral equation. Applying Green's second identity, a Fredholm integral equation of the second kind can be constructed as the follows:

$$2\pi\left\{\varphi_j^S\left(\boldsymbol{x}_j\right)\right\}_{l,q}+\iint_{S_B^j}\left\{\varphi_j^S\left(\boldsymbol{\xi}_j\right)\right\}_{l,q}\frac{\partial G\left(\boldsymbol{x}_j;\boldsymbol{\xi}_j\right)}{\partial n(\boldsymbol{\xi}_j)}\mathrm{d}S_{\boldsymbol{\xi}_j}=\iint_{S_B^j}V_{\mathrm{n}}(\boldsymbol{\xi}_j)G\left(\boldsymbol{x}_j;\boldsymbol{\xi}_j\right)\mathrm{d}S_{\boldsymbol{\xi}_j}. \tag{8.45}$$

Following Refs. [71, 239, 362], by applying Graf's addition theorem [820], it is straightforward to expand the free-surface Green function in the eigenfunction expansion and express it in polar coordinates in the form of

$$\begin{aligned}&G\left(\boldsymbol{x}_j;\boldsymbol{\xi}_j\right)=\\&2\pi iC_0\cosh k\left(z_j+h\right)\cosh k\left(\zeta_j+h\right)\sum_{m=-\infty}^{\infty}\left\{\begin{array}{l}H_m^{(1)}\left(kr_j\right)J_m\left(kR_j\right)\\H_m^{(1)}\left(kR_j\right)J_m\left(kr_j\right)\end{array}\right\}e^{\mathrm{i}m\left(\theta_j-\Theta_j\right)}+\\&4\sum_{n=1}^{\infty}C_n\cos k_n\left(z_j+h\right)\cos k_n\left(\zeta_j+h\right)\sum_{m=-\infty}^{\infty}\left\{\begin{array}{l}K_m\left(k_nr_j\right)I_m\left(k_nR_j\right)\\K_m\left(k_nR_j\right)I_m\left(k_nr_j\right)\end{array}\right\}e^{\mathrm{i}m\left(\theta_j-\Theta_j\right)},\end{aligned} \tag{8.46}$$

where the expansion coefficients are

$$C_0==\frac{k^2-K^2}{\left(k^2-K^2\right)h+K}=\frac{2k}{2kh+\sinh 2kh}, \tag{8.47}$$

$$C_n==\frac{k_n^2+K^2}{\left(k_n^2+K^2\right)h-K}=\frac{2k_n}{2k_nh+\sin 2k_nh}, \tag{8.48}$$

where $K=\omega^2/g$, and $k_n(n=0,1,2\ldots)$ are the roots of the wave dispersion equation in finite-depth water. In Eq. (8.46), the upper terms in the brackets are used when $r_j\geq R_j$ (the region outside of a circular cylinder that circumscribes the body or bodies) and the lower terms when $r_j<R_j$. The Green function in Eq. (8.46) was also named as the "ring source" by Ref. [362].

8.5.3 Removal of irregular frequencies

Similar to the wave interaction with a single floating body, directly solving Eq. (8.43) or Eq. (8.45) can lead to some unphysical numerical distortions in the computation results around the eigen-frequencies of the sloshing modes inside the floating body, which is normally termed the "irregular frequencies" phenomenon. For the source formulation, the "extended integral equation method" is recommended to remove the irregular frequencies, by adding a "rigid lid" at the interior waterplane section of the floating body. The boundary integral equations that need to be solved together are as below:

$$\begin{aligned}&2\pi\left\{\sigma_j^S\left(\boldsymbol{x}_j\right)\right\}_{l,q}+\iint_{S_B^j}\left\{\sigma_j^S\left(\boldsymbol{\xi}_j\right)\right\}_{l,q}\frac{\partial G\left(\boldsymbol{x}_j;\boldsymbol{\xi}_j\right)}{\partial n\left(\boldsymbol{x}_j\right)}\mathrm{d}S_{\boldsymbol{\xi}_j}+\\&\iint_{S_F^j}\left\{\sigma_j^W\left(\boldsymbol{\xi}_j\right)\right\}_{l,q}\frac{\partial G\left(\boldsymbol{x}_j;\boldsymbol{\xi}_j\right)}{\partial n\left(\boldsymbol{x}_j\right)}\mathrm{d}S_{\boldsymbol{\xi}_j}=V_{\mathrm{n}}\left(\boldsymbol{x}_j\right),\end{aligned} \tag{8.49}$$

$$-4\pi\left\{\sigma_j^S(\boldsymbol{x}_j)\right\}_{lq}+\iint_{S_B^j}\left\{\sigma_j^S(\boldsymbol{\xi}_j)\right\}_{l,q}\frac{\partial G(\boldsymbol{x}_j;\boldsymbol{\xi}_j)}{\partial n(\boldsymbol{x}_j)}\mathrm{d}S_{\boldsymbol{\xi}_j}+$$
$$\iint_{S_F^j}\left\{\sigma_j^W(\boldsymbol{\xi}_j)\right\}_{l,q}\frac{\partial G(\boldsymbol{x}_j;\boldsymbol{\xi}_j)}{\partial n(\boldsymbol{x}_j)}\mathrm{d}S_{\boldsymbol{\xi}_j}=V_{\mathrm{n}}'(\boldsymbol{x}_j)\,. \tag{8.50}$$

In Eq. (8.49) and Eq. (8.50), σ_j^W is the source strength on the waterplane area. The proper condition of the function V_{n}' has been discussed in Ref. [432]. Note that using this method, the logarithmic singularity should be subtracted from the Green function and then integrated analytically. For the potential formulation, it is recommended to use the "overdetermined integral equation method", as described in Refs. [592, 429, 454, 446], as it is not necessary to integrate the logarithmic singularity and sufficient accuracy can be achieved with only a few discrete points on the waterplane [446]. Using this method, the following additional equation needs to be solved together with Eq. (8.43):

$$\iint_{S_B^j}\left\{\varphi_j^S(\boldsymbol{\xi}_j)\right\}_{l,q}\frac{\partial G(\boldsymbol{x}_j;\boldsymbol{\xi}_j)}{\partial n(\boldsymbol{\xi}_j)}\mathrm{d}S_{\boldsymbol{\xi}_j}=\iint_{S_B^j}V_{\mathrm{n}}(\boldsymbol{\xi}_j)G(\boldsymbol{x}_j;\boldsymbol{\xi}_j)\,\mathrm{d}S_{\boldsymbol{\xi}_j}. \tag{8.51}$$

It should be noted in Eq. (8.51) that, the field point is taken from the discrete points on the interior waterplane area rather than those on the immersed body surface. Since the field point and the source point can never be coincident with each other, the diagonal terms with the solid angle coefficient diminish in Eq. (8.51), and the "irregular frequencies" can be effectively removed.

8.6 EVALUATION OF THE ARRAY PROPERTIES

8.6.1 Interaction factor and directionality

The interaction factor is a key metric to assess the performance of wave energy arrays. It is defined as

$$q(\beta)=\frac{\overline{P}_{\mathrm{array,max}}}{N_B\overline{P}_{\mathrm{isolated,max}}}, \tag{8.52}$$

where $\overline{P}_{\mathrm{array,max}}$ represents the maximum power absorbed by an array of N_B identical devices, $\overline{P}_{\mathrm{isolated,max}}$ represents the maximum power absorbed by a single such device in isolation, and β is the incident wave direction [839]. Eq. (8.52) means that if $q<1$, the average power per WEC in the array is less than the power of an isolated WEC [41]. Hence, wave interactions have a destructive effect on the power absorption of the wave farm. Conversely, if $q>1$, the park effect is constructive. Evans [209] and Falnes [224] independently derived the time-averaged power that can be absorbed by an array of oscillators in response to a regular wave train

$$\overline{P}_{\mathrm{array}}=\frac{1}{4}\left(\{U\}^*\{F^E\}+\{F^E\}^*\{U\}\right)-\frac{1}{2}\{U\}^*[B_{\mathrm{rad}}]\{U\}\}, \tag{8.53}$$

where $\{U\}$ and $\{F^E\}$ are the $N_B\times 1$ vectors of complex amplitudes of the body velocities and the wave excitation forces respectively; the asterisk $*$ denotes the complex conjugate transpose; and $[B_{\mathrm{rad}}]$ represents the $N_B\times N_B$ radiation damping matrix. The first term in Eq. (8.53) represents the total absorbed power from the incident

waves; whereas the second term is the power radiated back to the sea due to the motion of the bodies [508]. Provided $[B_{\text{rad}}]$ is positive definite, the maximum total absorbed power of the array can be derived as [209, 224]

$$\overline{P}_{\text{array,max}} = \frac{1}{8}\{F^E\}^*[B_{\text{rad}}]^{-1}\{F^E\}, \tag{8.54}$$

which occurs at the optimum condition

$$\{U\}_{\text{opt}} = \frac{1}{2}[B_{\text{rad}}]^{-1}\{F^E\}. \tag{8.55}$$

Under the assumption of point absorber theory, Ref. [243] proved the following variation relationship of q with respect to β for a fixed wave frequency:

$$\frac{1}{2\pi}\int_0^{2\pi} q(\beta)\mathrm{d}\beta = 1. \tag{8.56}$$

When neither point absorber theory nor optimised individual power take-off characteristics is used, Ref. [124] proposed an analogous consistency constant c:

$$c = \frac{1}{2\pi}\int_0^{2\pi} q(\beta)\mathrm{d}\beta. \tag{8.57}$$

Eq. (8.57) shows that when $c = 1$, the q-factor obeys the consistency condition.

By using the reciprocity relationship between the wave radiation damping and the wave excitation force [571], Ref. [839] proved that Eq. (8.56) holds for not only arrays of heaving axisymmetric devices but also for arrays of axisymmetric devices moving in uncoupled heave and surge or pitch degrees of freedom. For bodies with a vertical axis of symmetry, this leads to a result relating the capture width to the interaction factor [637, 243]:

$$\eta_{\text{array,max}} = \frac{\lambda}{2\pi}N_B q(\beta). \tag{8.58}$$

Equations (3.65) and (3.67) in Section 3.2.3.2, and Eq. (8.58) determine that the following relationship exists for an array of heaving point absorbers

$$q(\beta) = \frac{1}{N_B}\frac{\eta_{\text{array,max}}}{\eta_{\text{isolated,max}}}. \tag{8.59}$$

where $\eta_{\text{isolated,max}}$ is the maximum capture width of an isolated WEC. Eq. (8.59) illustrates that the interaction factor of an array of heave point absorbers can be evaluated as the ratio of the averaged capture width of the array to that of an individual device. Furthermore, it can be shown that a symmetry in the interaction factor with respect to the incident wave angle exists and is [522]

$$q(\beta) = q(\beta + \pi). \tag{8.60}$$

8.6.2 Overall energy production of the WEC array

Eq. (8.54) gives the maximum power of a WEC array at the optimum condition, i.e., Eq. (8.55). However, in many cases such an optimum condition is not satisfied. Assuming sinusoidal waves, the mean absorbed power of a generic WEC device over a wave period can be calculated as

$$\overline{P}_{\text{isolated}} = \frac{1}{T}\int_0^T B_{\text{pto}} U^2 \mathrm{d}t = \frac{1}{2}\omega^2 B_{\text{pto}} |U|^2, \tag{8.61}$$

The formulation can be extended to an array of multi-DoF WECs using the following matrix manipulation:

$$\overline{P}_{\text{array}} = \frac{1}{2}\omega^2 \sum_{j=1}^{N} \{U_j\}^T [B_{\text{pto},j}] \{U_j\}^*, \tag{8.62}$$

where j represents the j^{th} WEC converter; $\{U_j\}$ is an $M \times 1$ vector and $[B_{\text{pto},j}]$ is an $M \times M$ matrix; and M is the number of the total modes of each individual device. In many cases, when there is no coupling between the PTO systems of different DoFs in each individual WEC device, it is possible to formulate Eq. (8.62) as a summation of the non-zero terms given the majority of the elements in the PTO damping matrix are zeros, except for the diagonal terms. In such cases, Eq. (8.62) can be simplified as

$$\overline{P}_{\text{array}} = \frac{1}{2}\omega^2 \sum_{j=1}^{N}\sum_{i=1}^{M} B_{\text{pto}}^{j,i} |U_{j,i}|^2. \tag{8.63}$$

where i stands for the i^{th} mode in each individual device.

8.6.3 Case study

An idealised example is given here to illustrate how to evaluate the interaction factor $q(\beta)$ for a WEC array and verify the accuracy using the numerical method presented in this chapter. As shown in Figure 8.6, three heaving hemispherical point absorbers

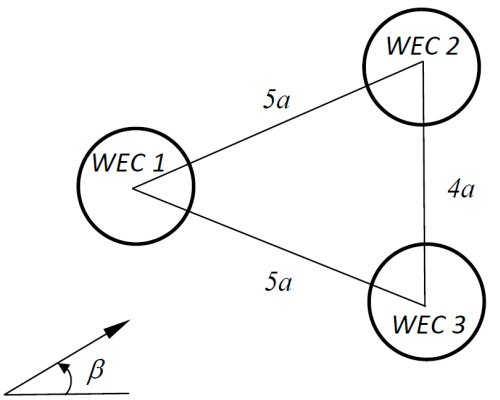

Figure 8.6: Plan-view layout of the three-device array configuration [839].

are displayed in an isosceles-triangle layout (Configuration B in Ref. [839]). The radius of each individual device is a and the water depth is $10a$. Half of each device is meshed by 2058 panels on its immersed hull and 331 panels on its waterplane area (taking advantage of the xoz symmetry plane). For heaving point absorbers, it is straightforward to derive the following expression from Eq. (8.59)

$$q(\beta) = \frac{2\pi}{\lambda N_B} \frac{\overline{P}_{\text{array,max}}(\beta)}{J}, \tag{8.64}$$

where $\overline{P}_{\text{array,max}}(\beta)$ can be evaluated by Eq. (8.54), and the average energy flux J can be evaluated by Eqs. (2.24) and Eq. (2.25) in Section 2.1.1.3, respectively.

The relationship between the interaction factor and the wave incident angle is plotted in Figure 8.7. The results are obtained using sufficient truncation numbers for the angular modes, as well as the wave number modes (see Eqs. 8.1–8.3, herein 10 terms are used for all the modes). It is found that, given a high wave number ka, this relationship varies dramatically with respect to the wave heading. The maximum value of q in the figure reaches 1.5, while the minimum approaches 0.6: both are at the extremes of the range. The results evaluated by the present method, based on interaction theory, exhibit good agreement with the results of Ref. [839]), which was evaluated by a complete boundary element method (quadratic polynomial approximation) for multiple-body interactions. Note that although a simple small array

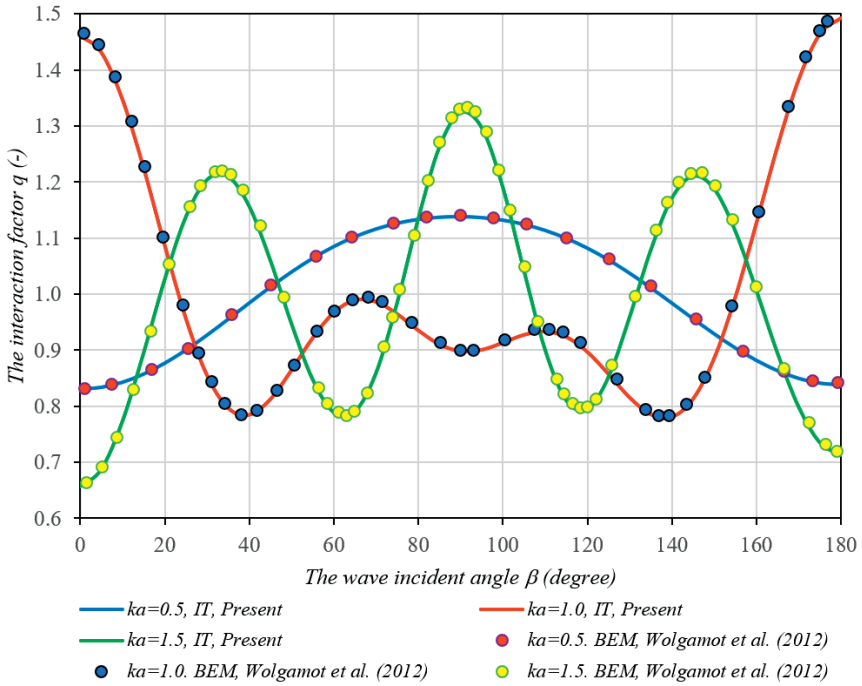

Figure 8.7: Plot of the interaction factor $q(\beta)$ against the wave incident angle β for an array of heaving hemispherical point absorbers in an isosceles-triangle layout (as indicated in Figure 8.6).

of three hemispherical point absorber WECs is shown for the case study here, the method itself can, in principle, be applied to large arrays of various WEC types with generic geometries.

8.7 SUMMARY

This chapter presents a sophisticated hybrid methodology combining the interaction theory of Kagemoto and Yue (1986) and the boundary element method. This new methodology successfully avoids evaluating the interactions between different bodies numerically, hence it is superior to the conventional boundary element method for wave interactions between multiple bodies in terms of computational efficiency. The general process of implementing the present methodology can be summarised as below. The diffraction transfer matrix, the radiation characteristics and the force transfer matrix are calculated by the BEM in advance for a single device in isolation. The total wave potential incident on each body is expressed as the summation of the ambient incident plane wave and all the scattered waves from other bodies. The wave potentials can be expanded as a Fourier series, in which the expansion coefficients are solved from the resultant linear algebraic system. Wave excitation forces, as well as added masses and radiation dampings, are then obtained by the product of the wave elevation and the force transfer matrix. Given the values of these quantities, the averaged capture width and the interaction factor of an array of WEC devices can finally be evaluated in a very straightforward manner. The case study of a simple array of hemispherical point absorbers provided at the end of the chapter illustrates the application in detail, and verifies the accuracy of the present methodology.